The Journal of Neuroscience, September 15, 1998, *18*(18):7436–7451

# Critical Role of Axonal A-Type $K^+$ Channels and Axonal Geometry in the Gating of Action Potential Propagation along CA3 Pyramidal Cell Axons: A Simulation Study

**Irina L. Kopysova**[1,2,3] **and Dominique Debanne**[1]

[1]*Unité de Neurocybernétique Cellulaire, UPR 9041 Centre National de la Recherche Scientifique, 13009 Marseille, France,* [2]*Innovationskolleg Theoretische Biologie, Humboldt-Universität zu Berlin, 10115 Berlin, Germany, and* [3]*Unité de Neurobiologie Expérimentale et Théorie des Systèmes Complexes, UPR 9081 Centre National de la Recherche Scientifique, 75231 Paris, France*

A model of CA3 pyramidal cell axons was used to study a new mode of gating of action potential (AP) propagation along the axon that depends on the activation of A-type $K^+$ current (Debanne et al., 1997). The axonal membrane contained voltage-dependent $Na^+$ channels, $K^+$ channels, and A-type $K^+$ channels. The density of axonal A-channels was first determined so that (1) at the resting membrane potential an AP elicited by a somatic depolarization was propagated into all axon collaterals and (2) propagation failures occurred when a brief somatic hyperpolarization preceded the AP induction. Both conditions were fulfilled only when A-channels were distributed in clusters but not when they were homogeneously distributed along the axon. Failure occurs in the proximal part of the axon. Conduction failure could be determined by a single cluster of A-channels, local decrease of axon diameter, or axonal elongation. We estimated the amplitude and temporal parameters of the hyperpolarization required for induction of a conduction block. Transient and small somatic hyperpolarizations, such as simulated $GABA_A$ inhibitory postsynaptic potentials, were able to block the AP propagation. It was shown that AP induction had to occur with a short delay (<30 msec) after the hyperpolarization. We discuss the possible conditions in which such local variations of the axon geometry and A-channel density may occur and the incidence of AP propagation failures on hippocampal network properties.

*Key words: hippocampus; modeling; conduction failure; neural networks; short-term plasticity; A-current*

The main function of the axon is to conduct action potentials (APs) from the cell body to the nerve terminals, thus allowing a spread of activity over long distances in the brain (Ramon y Cajal, 1911). When the AP fails to propagate along the axon, no signal can reach the output of the cell. Conduction failure thus represents a powerful filtering process that prevents communication with postsynaptic neurons. Three different modes of activity-dependent gating of AP propagation have been reported.

Conduction failures have been found in various types of neurons when APs are elicited at a frequency >10–30 Hz (Parnas, 1972; Bielefeldt and Jackson, 1993; Lüscher et al., 1994b). Such failures result from two factors: the presence of a low safety conduction point such as a branch point (Parnas, 1972; Grossman et al., 1979a; Lüscher et al., 1994a) or a bottleneck (Parnas et al., 1976), and accumulation of some ions (Grossman et al., 1979b; Smith, 1980; Bielefeldt and Jackson, 1993; Lüscher et al., 1994b, 1996). The second mode of gating is presynaptic inhibition (Nicoll and Alger, 1979; Wall, 1995). The main mechanism is a local depolarization or increase in the membrane conductance. It may either decrease the AP amplitude or block its conduction into the nerve terminal. For both types of gating, modeling studies have shown the importance of the local geometry of the axon (Parnas et al., 1976; Joyner et al., 1980; Lüscher and Shiner, 1990; Segev, 1990; Graham and Redman, 1994; Jackson and Zhang, 1995).

A novel form of gating that requires the activation of a fast A-type $K^+$ current has recently been reported in CA3 pyramidal cells *in vitro* (Debanne et al., 1997). Because A-channels are partly inactivated at the resting membrane potential (RMP) (Storm, 1990), conduction failure occurs only after a hyperpolarizing prepulse (Debanne et al., 1997). This conduction block depends on the recent activity of the cell and can be considered as a new form of short-term plasticity at the output side of the neuron.

Propagation failures were induced in only 30% of the cases (Debanne et al., 1997). Thus, A-current activation was necessary but not sufficient for conduction block, and additional factors such as distribution of the A-channels along the axon and/or the morphology of the axonal arborizations could play the role of a second gate. A-type $K^+$ channels have been found on axons of hippocampal pyramidal cells (Sheng et al., 1992; Maletic-Savatic, 1995), but their precise distribution remains unknown at the ultrastructural level. The density of these channels is regulated during early postnatal development (Maletic-Savatic, 1995), thus introducing variations in their distribution among cells. The topology and geometry of the axonal arborization also vary considerably in the population of CA3 pyramidal cells (Kosaka, 1980; Ishizuka et al., 1990). Because A-channel density and morphology of the axon may vary independently, simulations of realistic CA3

Received Feb. 23, 1998; revised June 24, 1998; accepted July 1, 1998.

This work was supported by Centre National de la Recherche Scientifique and Deutsche Forschungsgemeinschaft (I.L.K.) and a Fondation pour la Recherche Médicale grant (D.D.). We thank Drs. H. Bras, Y. Frégnac, B. H. Gähwiler, N. C. Guérineau, A. Herz, S. Korogod, T. Launay, and S. Tyc-Dumont for helpful discussions and constructive criticisms on this manuscript. We are particularly indebted to Professors B. H. Gähwiler and S. M. Thompson for collaboration on the experiments performed at the Brain Research Institute (University of Zurich, Switzerland) that are briefly reported here for comparison.

Correspondence should be addressed to Dr. Dominique Debanne, Unité de Neurocybernétique Cellulaire, UPR 9041 Centre National de la Recherche Scientifique, 280 Boulevard Sainte Marguerite, 13009 Marseille, France.

 0270-6474/98/187436-16$05.00/0

**Table 1. Morphological parameters of the structure**

| Branch no. | Diameter ($\mu$m) | Length ($\mu$m) | Number of compartments |
|---|---|---|---|
| 1 | 1.3 | 20 | 2 |
| 2 | 0.9 | 200 | 20 |
| 3 | 1.1 | 30 | 3 |
| 4 | 0.9 | 30 | 3 |
| 5 | 0.8 | 30 | 3 |
| 6 | 0.8 | 190 | 19 |
| 7 | 0.7 | 60 | 6 |
| 8 | 0.7 | 60 | 6 |
| 9 | 1.1 | 50 | 5 |
| 10 | 0.9 | 190 | 19 |
| 11 | 1.0 | 60 | 6 |
| 12 | 0.9 | 120 | 12 |
| 13 | 1.0 | 30 | 3 |
| 14 | 0.9 | 60 | 6 |
| 15 | 0.7 | 110 | 11 |
| 16 | 0.9 | 200 | 20 |
| 17 | 0.7 | 150 | 15 |

pyramidal cell axons offer a unique alternative to an experimental approach for studying A-channel-dependent block of AP propagation.

The first aim of this study was to simulate experimental gating of AP propagation. In a second step, we determined the incidence of local variations in A-channel density and in the morphology of CA3 pyramidal cell axons on AP conduction. We then estimated the minimal hyperpolarization required to induce a propagation block. Finally, we discussed which physiological hyperpolarization can provide favorable conditions for conduction failure.

The present experimental results have been published previously (Debanne et al., 1997) and are reported mainly for comparison with the results of simulations.

## MATERIALS AND METHODS

### *Experimental data*

Briefly, pairs of cells were recorded intracellularly in hippocampal slice cultures (Gähwiler, 1981). Monosynaptic connections between pairs of pyramidal cells were identified as reported previously (Debanne et al., 1995). As detailed earlier (Debanne et al., 1997), the postsynaptic cell was used as a detector of AP propagation in the presynaptic cell axon.

### *Morphology of the modeled cell*

The modeled structure included a soma, the principal axon, and main axon collaterals but was devoid of dendrites (see Fig. 2*B*). The axon was a reduced version of a CA3 pyramidal cell axon labeled *in vivo*, with geometrical parameters described by Li et al. [(1994), their Fig. 10]. The length of the principal axon was 450 $\mu$m. We did not consider all small distal collaterals. This structure, however, was large enough to reproduce experimental findings (see Results).

The cell body was presented as a cylinder with a length of 30 $\mu$m and a diameter of 25.5 $\mu$m. The somatic surface area (2402 $\mu m^2$) was identical to that in previous studies (Traub et al., 1994). The initial segment of the axon was a cylinder with a length of 40 $\mu$m and a diameter of 2.6 $\mu$m (Ishizuka et al., 1990). The axon of the cell was branched and unmyelinated, as reported for most of Schaffer collateral axons *in vivo* (Westrum and Blackstad, 1962; Andersen et al., 1978) and for hippocampal slice cultures (Frotscher and Gähwiler, 1988). Each branch was numbered from 1 to 17 (see Fig. 2*B*). The principal axon was made of branches 1, 3, 9, 11, 13, 14, and 16. The length and diameter of each axonal branch are shown in Table 1. Branch 1 corresponded to the area of AP initiation.

### *Biophysics of the modeled cell*

*Properties of simulated A-current.* Steady-state gating parameters of simulated A-current are shown in Figure 1*A*. The voltage dependence of activation and inactivation was abrupt, as reported for hippocampal neurons (Numann et al., 1987; Klee et al., 1995). At the RMP (Fig. 1*A*, *arrow*), a large portion of A-channels were inactivated, as shown in CA3 cells (Segal et al., 1984; Storm, 1990; Klee et al., 1995), and half of them were inactivated at approximately −70 mV (Segal et al., 1984).

Simulations reproduced the results of voltage-clamp experiments in the hippocampus *in vitro* with different characteristics of the hyperpolarizing prepulse (Segal et al., 1984; Numann et al., 1987; Storm, 1990; Klee et al., 1995). They showed how the amplitude of the preliminary hyperpolarization (Fig. 1*B*) and the interval between the hyperpolarization and the depolarization (Fig. 1*C*) modified the depolarization-induced activation of A-channels.

Because most channels are inactivated at rest, depolarization from the holding potential (−50 mV) produced only a small outward current (Fig. 1*B*). Hyperpolarization of the membrane by a step of voltage removed inactivation, and consequently allowed A-channel activation during membrane depolarization (Fig. 1*B*). The obtained current was sensitive to the level of the hyperpolarizing prepulse. Indeed, a 60 mV preliminary hyperpolarization led to a 4.6-fold increase in the amplitude of A-current.

To be effective, depolarization must closely follow hyperpolarization. Simulations were performed for different time intervals between the hyperpolarizing prepulse and depolarizing command pulse. Their results are shown in Figure 1*C*. The A-current was maximal when the depolarization immediately followed the hyperpolarization. Increasing the time interval between hyperpolarization and depolarization up to 50 msec led to twofold decrease in the amplitude of A-current.

*Distribution of ionic channels.* The somatic membrane contained voltage-dependent $Na^+$ channels, $Ca^{2+}$ channels, slow and fast $Ca^{2+}$-dependent $K^+$ channels, and delayed rectifier and A-type $K^+$ channels (Traub et al., 1991; Pongracz et al., 1992). The initial segment and axon contained neither $Ca^{2+}$ channels nor calcium-dependent $K^+$ channels (Traub et al., 1991; Pongracz et al., 1992). The density of $Na^+$ channels on the soma and the initial segment of the axon was close to that measured experimentally (Sah et al., 1988; Colbert and Johnston, 1996), and the parameter $G_{Na,max}$ (see Appendix, Eq. A4) was set to 50 mS/cm$^2$ as in previous studies (Pongracz et al., 1992). With such values of $G_{Na,max}$, the density of $Na^+$ current was found to be 9.5 pA/$\mu m^2$ when the protocol of patch-clamp experiments of Colbert and Johnston (1996) was simulated (i.e., membrane depolarization from −90 mV to −10 mV). The density of delayed rectifier $K^+$ channels was taken from patch-clamp estimations (Klee et al., 1995). Densities of $Ca^{2+}$ channels and $Ca^{2+}$-dependent $K^+$ channels on the soma were taken from the model of Pongracz et al. (1992). As suggested by the findings of Colbert and Johnston (1996), the area of AP initiation was distal to the initial segment. In this region, 20 $\mu$m long and 40 $\mu$m from the soma, $Na^+$ channel density was 30 times those of the initial segment and the soma, in agreement with theoretical studies (Rapp et al., 1996) and recent experiments (Dargent et al., 1998). The density of delayed rectifier $K^+$ channels was increased correspondingly. The densities of $Na^+$ and $K^+$ channels in the rest of the axon were the same as in the soma. Channel densities in the cellular compartments are listed in Table 2.

*Distribution of A-channels.* In the model, a parameter of A-channel density, $G_A$, was expressed as a function of the maximal conductance $G_{A,max}$: $G_A = G_{A,max} \cdot a \cdot b$, where $a$ and $b$ are the variables of activation and inactivation, respectively (see Appendix and Fig. 1*A*). In patch-clamp experiments, the density of A-current in the soma of CA3 pyramidal neurons has been found to vary between 0.055 and 0.377 mA/cm$^2$ (Klee et al., 1995). To cover this range, we considered three values of $G_{A,max}$: 4, 4.05, or 4.1 mS/cm$^2$. With such values, the densities of A-current measured at a membrane potential of +30 mV after a hyperpolarizing prepulse to −110 mV were 0.308, 0.313, and 0.316 mA/cm$^2$, respectively. The area of AP generation had a maximal density of 4.1 mS/cm$^2$. Because the distribution and density of A-type $K^+$ channels have not been characterized with high precision in axons of CA3 pyramidal cells, we considered two distributions of A-channels along the axon: (1) homogeneous distribution with a density ($G_{A,max}$) from 0.5 to 5 mS/cm$^2$; and (2) heterogeneous distribution with hot spots at the branch points, covering 20 $\mu$m on both sides of each bifurcation ($G_{A,max}$ = 4, 4.05, or 4.1 mS/cm$^2$) and low density of A-channels between the bifurcations ($G_{A,max}$ = 1.2 mS/cm$^2$). Such reductions in the density correspond to the removal of five A-channels in every hot spot. Estimations of the number of channels were based on the voltage-clamp mea-

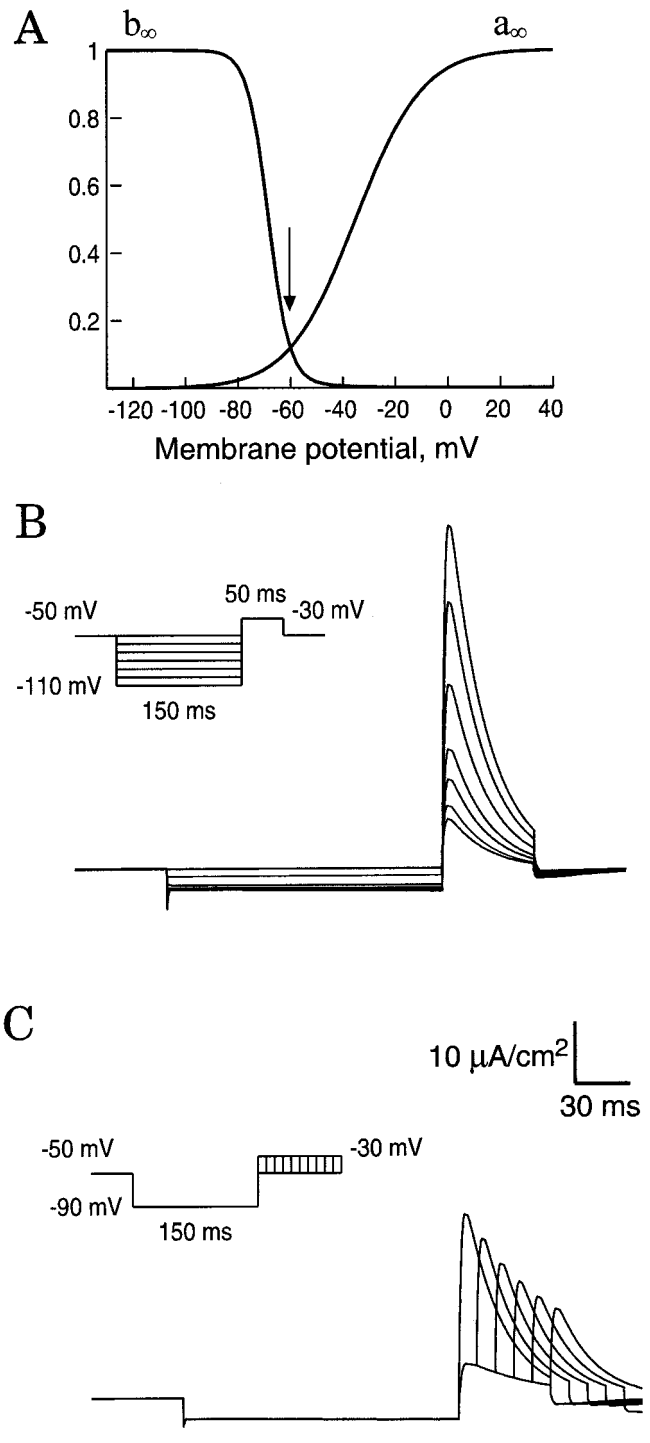


*Figure 1.* Properties of A-current in an isolated compartment of membrane. *A*, Activation and inactivation curves of A-current. Note that at the RMP (*vertical arrow*), most of the channels were inactivated. *B*, Level of the hyperpolarization and recovery from inactivation in simulations of voltage-clamp-mode experiments. The holding potential was −50 mV. A-current was activated after a 150 msec hyperpolarizing prepulse by the depolarizing pulse to +30 mV (50 msec duration). Hyperpolarizing voltage command ranged between −50 and −110 mV (*inset*). A-current increased significantly with the level of the hyperpolarization. *C*, Delay between the hyperpolarizing prepulse and depolarizing command. The membrane was hyperpolarized to −90 mV during the prepulse. The depolarizing command (+30 mV) was applied 0, 10, 20, 30, 40, and 50 msec after the end of the hyperpolarization (*inset*). The shorter the delay of delivery of the depolarization, the larger the peak of A-current.

**Table 2. Distribution of ionic channels**

| | $G_{max}$ | | | | | |
|---|---|---|---|---|---|---|
| | $Na^+$ | $K^+$ | $Ca^{2+}$ | $K_{Ca}$ | $K_C$ | $K_A$ (mS/cm$^2$) |
| Soma | 50 | 50 | 0.2 | 1 | 1 | 4.1 |
| Initial segment | 50 | 50 | 0 | 0 | 0 | 4.1 |
| Area of spike generation | 1500 | 1500 | 0 | 0 | 0 | 4.1 |
| Axon | 50 | 50 | 0 | 0 | 0 | 1.2 (at bifurcations 4.0, 4.05, or 4.1) |

surements of single-channel A-current in CA3 pyramidal cells in organotypic slice culture (Bossu et al., 1996).

*Computations.* The simulations were based on numerical solutions of the cable equation (see Appendix). Transmembrane ionic currents were described by models published earlier (Traub et al., 1991; Pongracz et al., 1992). Each current was described by a Hodgkin-Huxley type equation. Details on equations and values of their parameters are provided in the Appendix. Voltage-clamp simulations (Fig. 1) were performed with the software PATCH (Kopysova and Korogod, 1989), especially designed for a single membrane compartment. Simulations of AP propagation were performed with the software CRONA (Korogod, 1989; Korogod et al., 1991) based on the equations and numerical method described in Korogod et al. (1994). Integration time step was 1 μsec; the length of each equipotential compartment of the simulated structure was 10 μm. The number of compartments for each axonal branch is shown in Table 1. All computations were done on IBM Pentium Pro 200 computer.

## RESULTS

### Propagation of the AP elicited from RMP

We first determined the configuration of the model that allowed successful propagation of the AP into all axonal collaterals under inactivation of the A-current (i.e., at the RMP).

We considered homogeneous distribution of A-channels along the whole axon. The parameter $G_{A,max}$ varied between 0.5 and 5 mS/cm$^2$ (Fig. 2*A*). AP elicited by a somatic depolarizing step of current was successfully propagated into all axon branches when $G_{A,max}$ was set up to 2.5 mS/cm$^2$ (Fig. 2*A,B*). When A-channel density had been increased to 2.6 mS/cm$^2$, AP failed in several branches [12 and 16 (Fig. 2*A,C*)]. The number of axon collaterals exhibiting failures increased with A-channel density. With $G_{A,max}$ of 4.5 and 5 mS/cm$^2$, the AP was still initiated at the area of AP generation but did not reach any terminal (Fig. 2*A*).

AP propagation from the cell body to all nerve terminals was also successful when hot spots of A-channels ($G_{A,max}$ = 4.1 mS/cm$^2$) at the branch points were added to homogeneously ($G_{A,max}$ = 1.2 mS/cm$^2$) distributed A-channels (Fig. 2*D*). The presence of the hot spots of A-channels at the bifurcations decreased the AP amplitude at the branch point between branches 9 and 11 (Fig. 2, compare *B,D*). The AP, however, was able to recover and propagate actively into all axon terminals.

### AP propagation after a somatic hyperpolarization

Propagation of the AP elicited after a hyperpolarizing prepulse was tested in the two configurations that allowed a successful propagation from the RMP [i.e., homogeneous density with $G_{A,max}$ = 2.5 mS/cm$^2$ (Fig. 2*B*), and clustered distribution (Fig. 2*D*)]. The configuration that did not allow successful propagation from the RMP ($G_{A,max}$ = 2.6 mS/cm$^2$) was discarded.

The AP was elicited after a hyperpolarizing current prepulse applied at the soma (Fig. 3*A,B*). The delay between the onset of the depolarizing step of the current and the spike was 1.2 msec. With homogeneously distributed A-channels, the AP propagated

into all terminals, although locally (in branches 9, 11, and 13) the amplitude of the AP was reduced (Fig. 3*A*). The propagation failure was not possible to obtain even when the hyperpolarization was increased to −40 mV (data not shown). In contrast, AP failures were observed in the principal axon (branch 16) and collateral 12 when hot spots of A-channels were at the branch points (Fig. 3*B*). It is important to note that the AP was normally propagated into branches 2, 7, and 10. This differential propagation into axonal collaterals well matched the experimental results in the hippocampal slice cultures (Fig. 3*C*) where the hyperpolarization was able to block the coupling between neurons 1 and 2 but not 1 and 3 (Fig. 3*C*) (Debanne et al., 1997).

### Determination of the location of propagation failure

The location of AP failure is very difficult to determine experimentally because it would require multiple electrophysiological recordings from the axon. These recordings can be performed in large crustacean axons (Grossman et al., 1979a) but not in thin mammalian axons. At the moment, only the modeling approach allows estimations of this area.

A-channels are inactivated at the RMP. To produce a propagation block, A-channels have to recover from inactivation. This can be achieved only if axonal membrane is hyperpolarized (Fig. 1*B*). Therefore it is important to determine how far in the axon a somatic hyperpolarization can be spread electrotonically.

The model showed that a steady-state somatic hyperpolarization of 9.5 mV applied at the soma attenuated along the principal axon within the first 200 μm (Fig. 4*A*). Downstream from the first bifurcation point (100 μm), the level of the hyperpolarization was already attenuated by almost 50%. Only 8.5% of the hyperpolarization remained behind the third bifurcation. Hyperpolarization was attenuated almost completely at 240 μm (210 μm from the soma), suggesting that AP failure could occur only along this proximal part of the axon.

To determine the location of the conduction failure more precisely, we compared the amplitudes of the AP, A-currents, and $Na^+$ currents in the soma (Fig. 4*B*) and at four points along the proximal part of the principal axon (Fig. 4*C*). Simulations were performed with and without the hyperpolarizing prepulse. Because the level of the hyperpolarization in the very proximal area was only slightly attenuated (Fig. 4*A*), the preliminary hyperpolarization drastically increased the A-current (26% at the area of spike generation) (Fig. 4*C*, first recording point). This increase, however, had only a small influence on the amplitude of the AP because of the high density of $Na^+$ channels in this area, which were also deinactivated by the hyperpolarization (see $Na^+$ currents in Fig. 4*C*). Compared with control, a delay of ~1 msec in the generation of the AP was observed. Downstream from the first bifurcation point (Fig. 4*C*, second recording point), somatic hyperpolarization was still able to significantly increase the A-current (up to 14%). The proximity of the area of the AP initiation kept the amplitude of the AP almost unchanged. Reduction of ~1 mV in the AP amplitude was found at this level. Farther away from the area of the spike generation, the hyperpolarization-induced increase in the A-current played a more important role. Behind the second bifurcation (Fig. 4*C*, third recording point), the small increase in the A-current (only 7%) led to a 1.5 mV reduction in the AP amplitude. The AP was dramatically attenuated between second and third bifurcation (Fig. 4*C*, fourth recording point). Indeed, behind the third bifurcation, the AP amplitude was 8 mV smaller than under control conditions (oblique arrow).

We conclude that propagation failure occurred in the axonal branches that meet two conditions. First, the area must still be under the influence of the somatic hyperpolarization and therefore be proximal. Second, it must be remote from the area of high density of $Na^+$ channels so that the effect of the A-current expresses. In other words, the failure occurred in the axonal region where the potassium inhibition dominated the sodium activation. In the next experiments, we studied how the modifications in the density of A-channels and in the axonal geometry affected the AP propagation.

### Single clusters of A-channels determine propagation failure

We first tested the consequences of removing a single proximal hot spot of A-channels on the conduction properties. To examine this question, we used the configuration illustrated in Figure 3*B* (and reproduced by a *dashed line* in Fig. 5). Because the area between the second and third branch points was a region of low safety for AP propagation, we chose to remove the hot spot at the second branch point (indicated by a dashed circle). When the hot spot was removed, the AP was conducted successfully to the end of the principal axon (Fig. 5).

These results show that A-channel activation is required for AP conduction to be blocked and that a single cluster of A-channels in the area of AP failure might influence the AP propagation along the axon (see Discussion).

### Role of the axonal morphology

In a second step, we tested the consequences of geometrical modifications within the proximal part of the axon. In organotypic slice cultures, propagation failures were found in approximately one-third of CA3 pyramidal cell axons (Debanne et al., 1997). One possible explanation is that the general pattern of the proximal arborization of the axon varies considerably in the population of CA3 neurons (Kosaka, 1980; Ishizuka et al., 1990). Two factors cause this variation: the length of each segment between two consecutive branch points, which may vary by a few tens of micrometers (Kosaka, 1980; Ishizuka et al., 1990), and the diameters of the parent and daughter collaterals, which vary between 0.6 and 1.6 μm (Ishizuka et al., 1990). We therefore tested the effect of each of these parameters on propagation failure. We again considered the configuration shown in Figure 3*B* (repeated in Fig. 6*A*). Modifications of the axon morphology were limited within the proximal part of the axon, which was of low safety for AP propagation.

When the length of branch 9 (limited by branch points a and b) was increased by 50 μm, propagation failures were suppressed (Fig. 6*B*). Similarly, conduction was successful in the whole axonal tree when the axon diameter was reduced by 0.1 μm in the axonal branches labeled by × (Fig. 6*C*).

Time courses of the AP were calculated for each 10 μm along branches 3 and 9, and along the first 20 μm of branches 10 and 11. AP amplitudes were measured and compared for the three configurations in Figure 6. Close to the area of AP initiation (70 μm from the soma), AP amplitudes were identical in all configurations (Fig. 7). Under control conditions (black triangles), the amplitude of the AP decreased along the axon, with larger gradients at the vicinity of each branch point (a and b). Behind the second branching point (150 μm), the difference in the AP amplitudes in branches 10 and 11 was ~4 mV. AP was sufficiently high to activate $Na^+$ channels in the right branch (10) but not in the left (11).

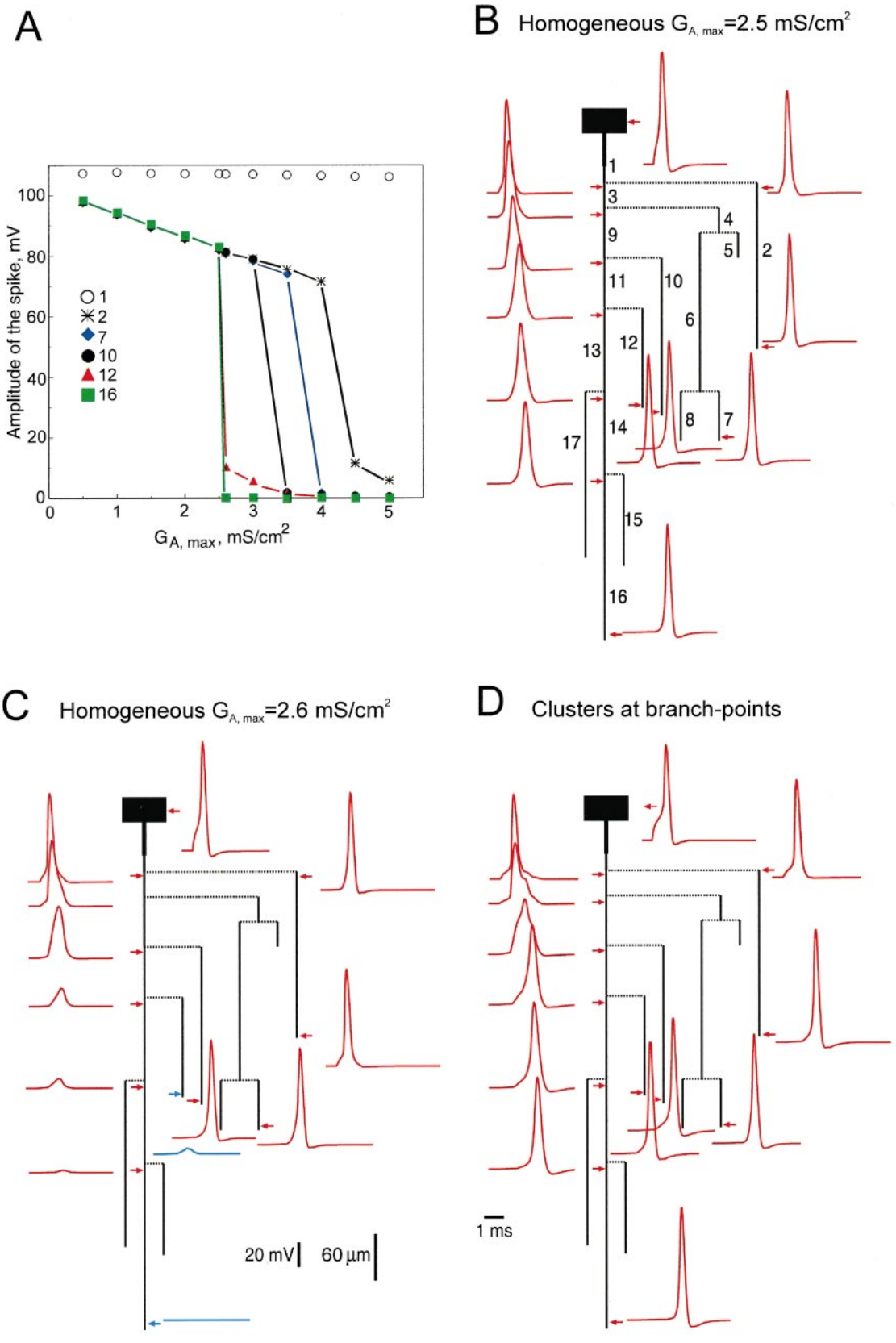


*Figure 2.* Propagation of the AP along the axon with different distributions of A-channels. *A*, Homogeneous distribution. Amplitudes of the AP in the area of the spike generation (branch 1) and in five axonal collaterals (2, 7, 10, 12, and 16; see *B*) as a function of the density of A-channels. At low density ($G_{A,max} \leq 2.5$ mS/cm$^2$), the AP propagated into all axonal terminals. At $G_{A,max} = 2.6$ mS/cm$^2$ conduction failed in branch 16 of the principal axon and collateral 12 was obtained. With further increase of $G_{A,max}$, more terminals were blocked, and at $G_{A,max} = 4.5$ mS/cm$^2$ the AP failed to reach any terminal. *B*, Details of AP propagation within the whole axonal arborization when A-channels were distributed homogeneously (*Figure legend continues*)

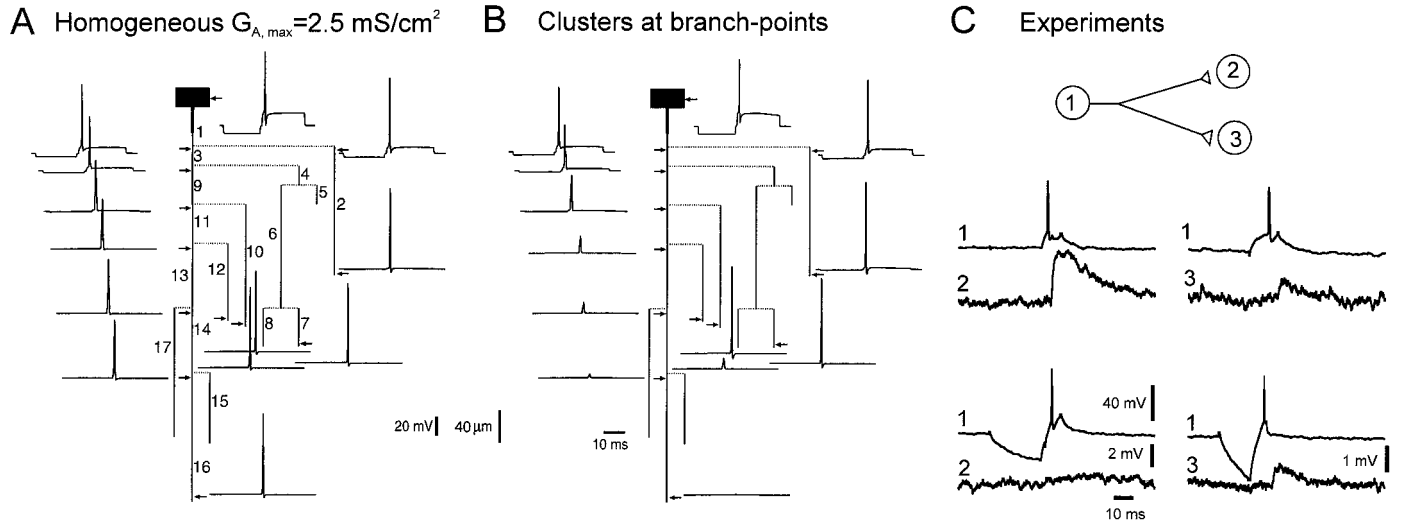


*Figure 3.* Propagation of the AP after a hyperpolarizing prepulse. *A*, Simulations for homogeneous distribution of A-channels ($G_{A,max}$ = 2.5 mS/cm$^2$). AP was elicited after a 20 msec hyperpolarizing prepulse of 9.5 mV. No conduction failure was induced. *B*, Clustered distribution as in Figure 2*D*. The same hyperpolarization induced propagation failures along the principal axon (branch 16) and collateral 12 but not in adjacent collaterals (2, 7, and 10). *C*, Selective conduction block in CA3 cells of hippocampal slice cultures. Pairs of two monosynaptically CA3 pyramidal cells were recorded intracellularly. Presynaptic AP induced in the cell (*1*) at the RMP evoked an EPSP in cell (*2*). When cell (*1*) was phasically hyperpolarized, no EPSP was elicited in the cell (*2*). The electrode was then removed from the cell (*2*) and inserted in the cell (*3*). Even in the presence of phasic hyperpolarization, the presynaptic AP always evoked an EPSP. AP thus failed in the axonal collateral of cell (*1*) to cell (*2*), but not in the branch to cell (*3*).

In contrast with the control situation, the AP amplitude was locally preserved when the axon was elongated between a and b (empty circles). In this configuration the branching point b was replaced by b'. The distance between two successive clusters of A-channels (at a and b') was increased. After the first bifurcation (100–140 $\mu$m), the AP amplitude increased and then progressively decreased while approaching the second bifurcation (b'). The AP was able to propagate into both the principal axon (11) and the collateral (10).

When the axon diameter was decreased (filled circles) in the branch between the bifurcations a and b, the input impedance increased by 15%. As a result, when the AP reached the bifurcation a, its amplitude was less attenuated than in control (black triangles). Behind the bifurcation b, APs in both daughter branches were sufficiently high to allow active propagation up to the end of these collaterals.

In all cases, the amplitude of the AP in branch 11 was smaller than in 10 because of the proximity of the next bifurcation (see the whole structure in Fig. 6).

## Required minimal amplitude and duration of the hyperpolarization for conduction block

Physiological hyperpolarizations are limited in both duration and amplitude by several factors, such as the kinetics of transmitter release, access, degradation or buffering of the second messengers, kinetics of activation and inactivation of the channels involved, and the equilibrium potentials of the ions that flow through the channels.

To know whether physiological hyperpolarizations suffice to induce a conduction block, we estimated the minimal duration and amplitude of a current-induced hyperpolarization to produce a conduction failure. In addition to the $G_{A,max}$ = 4.1 mS/cm$^2$ used before, we considered two other densities of A-channels in the hot spots: $G_{A,max}$ = 4 and 4.05 mS/cm$^2$.

As expected from inactivation properties of the A-channels, the level required for hyperpolarization was lower for larger durations of the hyperpolarization (Fig. 8*B*). For example, when the A-channel density at the branch points was 4.05 mS/cm$^2$, a 10 msec hyperpolarization had to be as large as −72 mV to block the conduction. The required hyperpolarization decreased to less than −64 mV when the duration was increased to 30 msec. For all densities, the curves reached a plateau for durations larger than 40 msec. This saturation is a consequence of the deinactivation of A-current, achieved within 50–100 msec (Storm, 1990; Klee et al., 1995). When the density of A-channels was decreased from 4.1 to 4.05 and 4.0 mS/cm$^2$, larger hyperpolarizations were required. The amplitude of the required hyperpolarization was found to be very critical. For a duration of 20 msec, the required hyperpolarization increased from −63 mV to −66.5 and −76 mV when $G_{A,max}$ decreased from 4.1 mS/cm$^2$ to 4.05 and 4 mS/cm$^2$, respectively.

Because $G_{A,max}$ = 4.1 mS/cm$^2$ was found to provide a conduction block even with very small levels of hyperpolarization, we used a smaller value of $G_{A,max}$ (4.05 mS/cm$^2$) in the next computations.

## Role of the delay between the hyperpolarization and AP induction

In all previous examples, depolarizing currents were applied with a fixed delay of 1 msec after the offset of the hyperpolarizing

←

with a low density ($G_{A,max}$ = 2.5 mS/cm$^2$). Action potentials were elicited by a brief current-induced depolarization (inflection on the rising phase of the AP). *C*, Propagation failed in the principal axon (16) and in the collateral 12 (*blue traces*) when A-channel density was increased to 2.6 mS/cm$^2$. *D*, Successful propagation when hot spots of A-channels ($G_{A,max}$ = 4.1 mS/cm$^2$) at the branch points were added to a low homogeneous density of A-channels ($G_{A,max}$ = 1.2 mS/cm$^2$).

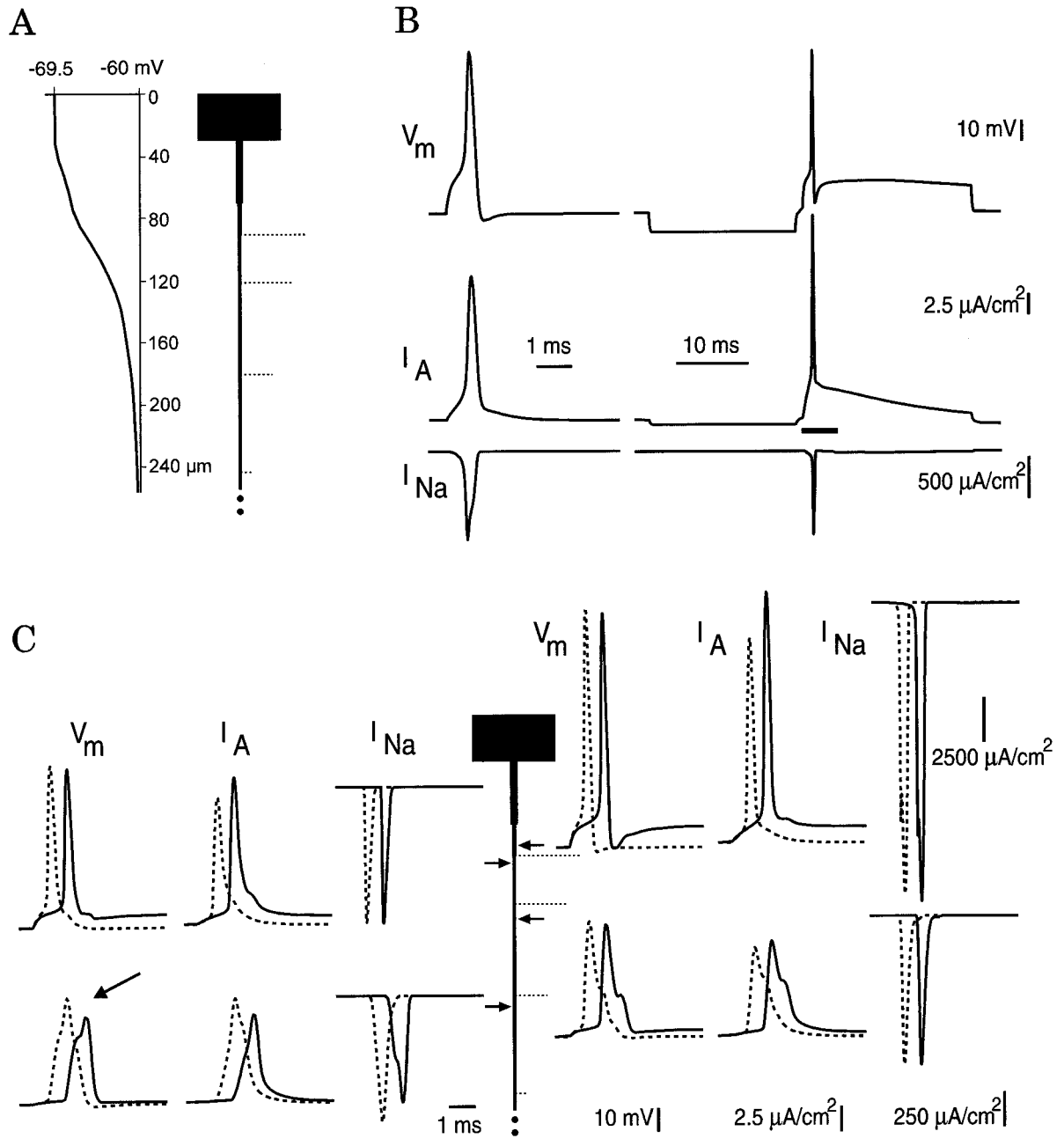


*Figure 4.* Location of the AP failure along the principal axon. *A*, Electrotonic attenuation along the principal axon of a steady-state hyperpolarization to −69.5 mV induced at the soma. Note that downstream from the third branch point (>200 μm), the membrane was almost not polarized. *B*, Time courses of the membrane potential in the soma ($V_m$, *top*) and densities of A-current ($I_A$, *middle*) and $Na^+$ current ($I_{Na}$, *bottom*) in response to a depolarization elicited either from the RMP (*left*) or after the hyperpolarizing prepulse (*right*). *C*, Time courses of the membrane potential ($V_m$, *left*) and densities of the A-current ($I_A$, *middle*) and $Na^+$ current ($I_{Na}$, *right*) were compared along the axon without (*dashed lines*) and with a hyperpolarizing prepulse (*solid lines*). All signals have been expanded over a duration of 5.5 msec (*B, horizontal bar*). Note the difference in the vertical scales for the $Na^+$ currents in the soma (*B*), in the area of spike initiation, and in the rest of the axon.

current. We examined the role of this delay on AP conduction along the principal axon (Fig. 9). For these computations, the amplitude of the hyperpolarization at the soma was set to 30 mV. For small delays of 1–25 msec (Fig. 9*A,B*), no signal reached the terminal of the principal axon. AP propagation was successful, however, when the delay was increased to 35 msec (Fig. 9*C*). Similarly, for a delay of 25 msec, propagation recovered when a short subthreshold depolarization (5 msec, 4.4 mV) followed the hyperpolarizing prepulse (Fig. 9*D*). In all cases, the time course of A-current was calculated (Fig. 9*A–D*, *second trace*). The amplitude of A-current decreased when the delay was increased (Fig. 9*E*). At 25 msec, this amplitude was much smaller when the subthreshold depolarization was added.

Similar critical values were observed in experiments [Fig. 9*F* and Debanne et al. (1997)]. If a brief hyperpolarizating pulse of current was applied 15 msec before AP induction, no EPSP was observed (Fig. 9*F*, *top*). When the interval between the end of the hyperpolarizing prepulse and the induction of the AP was in-

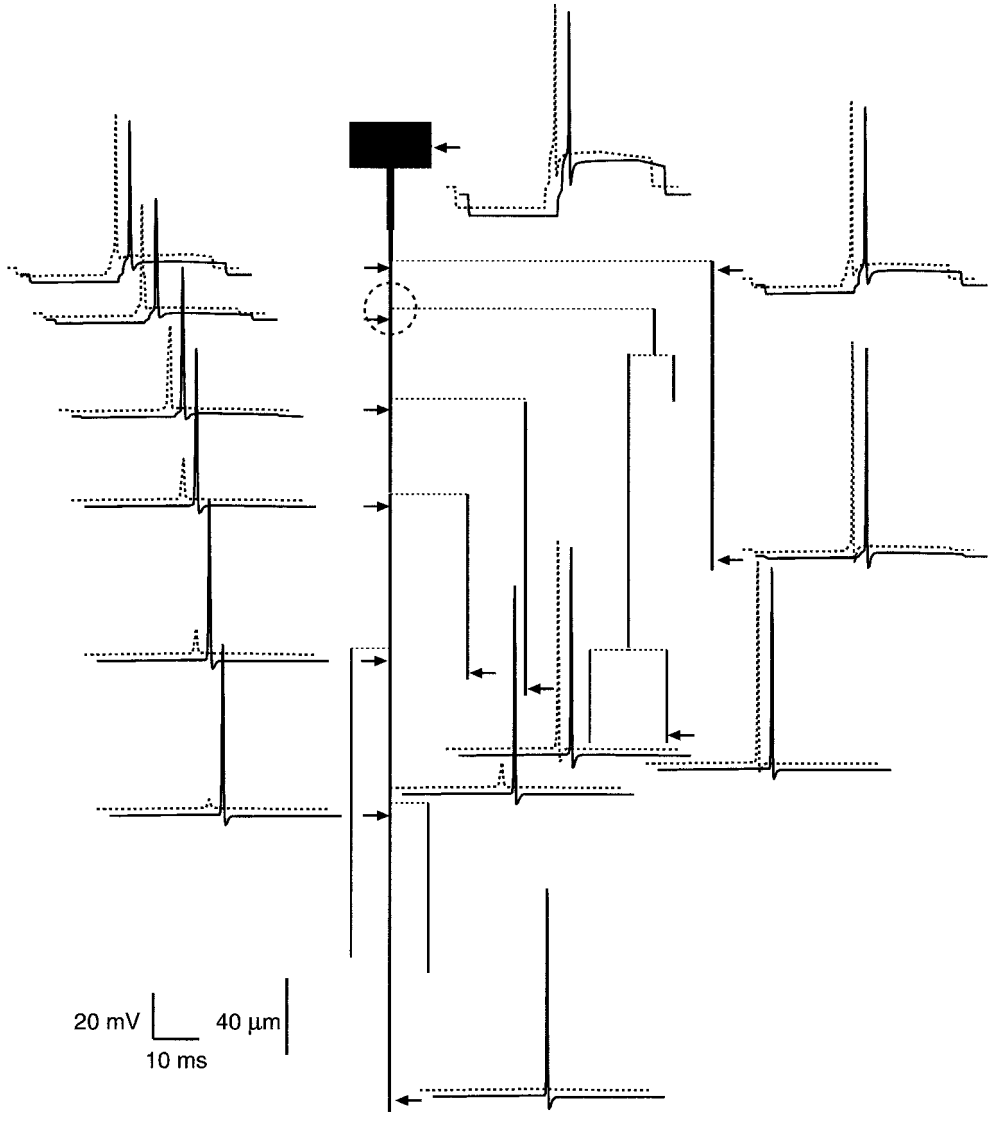


*Figure 5.* Effect of removal of a single cluster on propagation failure. The control configuration was indicated by a *dashed line*. When the cluster of A-channel was removed from the second branch point (indicated by the *dashed circle*), the AP propagated successfully into all axon terminals (*solid line*).

creased to 35 msec, then the prepulse did not prevent an EPSP from being elicited (Fig. 9*F*, *bottom*).

### AP propagation block after $GABA_A$ IPSPs

The preceding computations showed that relatively small hyperpolarizations were able to block the AP conduction in the axon. We therefore tested whether a simulated $GABA_A$ IPSP of small amplitude would block AP propagation. In the absence of any IPSP, the AP reached both the end of the collateral (Fig. 10*A*, trace *2*) and the principal axon (Fig. 10*A*, trace *3*). A somatic $GABA_A$-like IPSP of 5.5 mV was generated at the soma by an increase in $Cl^-$-conductance with the profile of an $\alpha$-function (Fig. 10*B*, *trace 1*). Because of a fast attenuation along the principal axon, the IPSP did not influence the membrane potential at the terminals (Fig. 10*B*, *traces 2* and *3*). A selective failure in the principal axon (Fig. 10*C, trace 3*) but not in the collateral (Fig. 10*C, trace 2*) was obtained when the AP was evoked after the onset of the simulated IPSP (Fig. 10*C*).

Comparable conduction block was observed experimentally [Debanne et al. (1997); Fig. 10*D*]. In control conditions (at the RMP), each presynaptic AP evoked a postsynaptic response (data not shown). No postsynaptic event was evoked, however, when the presynaptic AP was elicited after a hyperpolarizing prepulse of current; this indicated that propagation failure was induced (Fig. 10*D*, *top left*). Similarly, the presynaptic AP failed to produce a response when the current-induced hyperpolarization in the presynaptic cell was replaced by a compound IPSP (Fig. 10*D*, *top right*). Postsynaptic responses were observed for both current-induced and synaptically induced hyperpolarizations when the delay between the end of the hyperpolarizing prepulse and the AP induction was increased up to ~30 msec (Fig. 10*D*, *bottom*). We conclude that physiological hyperpolarizations such as $GABA_A$ IPSPs are sufficient to block AP propagation elicited in a time window of <30 msec before AP induction.

### Density and kinetics of $Na^+$ channels

Because the exact measurements of density and kinetic properties of $Na^+$ channels in the axons of the hippocampal pyramidal neurons are lacking, it was important to study how the model behavior depends on the parameters of $Na^+$ channels.

In the first set of experiments we varied the density of $Na^+$ channels (parameter $G_{Na,max}$) on the soma and along the axon around the value of 50 $mS/cm^2$ used in previous simulations. The maximum density of A-channels in the bifurcation hot spots

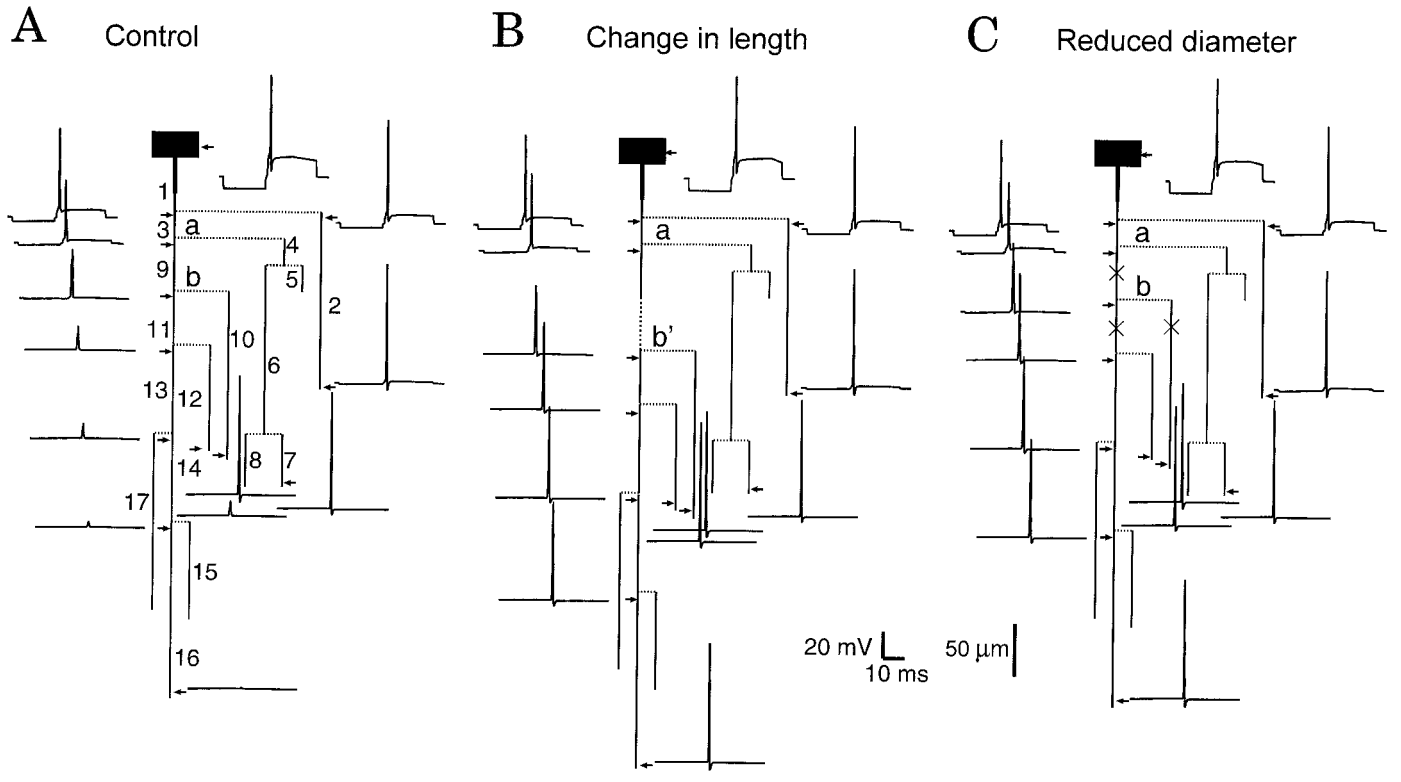


*Figure 6.* Effect of axon elongation and reduction of the axonal diameter on propagation failure. *A*, Control configuration. *B*, The length of axonal branch 9 was increased from 50 (*a, b* in *A*) to 100 μm (*a, b'* in *B*). As a result, the AP propagated into all axonal collaterals. *C*, The diameter was decreased by 0.1 μm in three branches labeled by × (9, 10, and 11). Propagation into the whole axonal arborization was achieved.

(parameter $G_{A,max}$) that allowed the successful propagation into all axonal terminals at the RMP was determined for each value of $G_{Na,max}$. The values of the maximum possible $G_{A,max}$ in the hot spots as function of the density of $Na^+$ channels are presented in Figure 11*A* (*top*). For $G_{Na,max}$ lower than 35 mS/cm$^2$, the AP failed to propagate into some axonal terminals even when hot spots were suppressed and A-channels were homogeneously distributed ($G_{A,max}$ = 1.2 mS/cm$^2$) along the whole axon. With an increase of $G_{Na,max}$ the maximal possible density of A-channels increased almost linearly. Ratio $G_{Na,max}/G_{A,max}$ was calculated for different $G_{Na,max}$ and presented in Figure 11*A* (*middle*). It was suggested that both successful propagation at the RMP and hyperpolarization-induced block of spike propagation could be obtained more easily at higher density of $Na^+$ channels when the ratio $G_{Na,max}/G_{A,max}$ was higher. Results of the estimations of the hyperpolarization required for conduction failure into the principal axon are presented in Figure 11*A* (*bottom*). One can notice from the comparison of the middle and bottom of Figure 11*A* that the required level of the hyperpolarization was determined by the ratio $G_{Na,max}/G_{A,max}$. For $G_{Na,max}$ = 35 mS/cm$^2$, when $G_{Na,max}/G_{A,max}$ was 16.5, the required hyperpolarization was −118 mV. This level of the hyperpolarization cannot be reached during normal neuronal activity. For $G_{Na,max}$ = 40 mS/cm$^2$, the ratio $G_{Na,max}/G_{A,max}$ was lower and equaled 12.1. In this case, the required level of the hyperpolarization was only −72 mV. Such level of hyperpolarization is physiologically possible and may correspond to that reached during an IPSP or an afterhyperpolarization (AHP). For $G_{Na,max}$ in the range of 45–60 mS/cm$^2$, the ratios $G_{Na,max}/G_{A,max}$ were almost the same, and the required levels of the hyperpolarization were similar.

In the next set of simulations, we studied the role of the kinetic properties of $Na^+$ current. We considered the cases when the time constants of both activation and inactivation of $Na^+$ channels were multiplied by a scale factor ranging from 0.1 to 2. The results of simulated propagation of the AP into five axonal terminals for different kinetics of $Na^+$ channels are presented in Figure 11*B*. For all considered kinetics, a somatic depolarizing step of current induced generation of the AP in the area of spike generation in the axon (Fig. 11*B*, *open circles*). The AP successfully propagated into all axon terminals when time constants were multiplied by a scale factor ranging from 1 to 2. When the kinetics of $Na^+$ channels were accelerated (multiplied by a scale factor ranging from 0.4 to 0.9), AP propagation failed in several branches (10, 12, and 16). The number of axon collaterals exhibiting conduction failure increased with further acceleration of the $Na^+$ channel kinetics. When time constants of activation and inactivation of $Na^+$ channels were decreased tenfold, the AP was still initiated at the area of AP generation but did not reach any terminal (Fig. 11*B*).

The level of the hyperpolarization required for conduction failure was influenced only slightly when the time constants of activation and inactivation of $Na^+$ channels were increased two times. For both control and twofold slower $Na^+$ kinetics, propagation failure in the principal axon was observed when a 20 msec hyperpolarizing prepulse of 6 mV preceded the AP (data not shown).

## DISCUSSION

We provide theoretical evidence that axonal A-current can be deinactivated by somatic hyperpolarization in the physiological

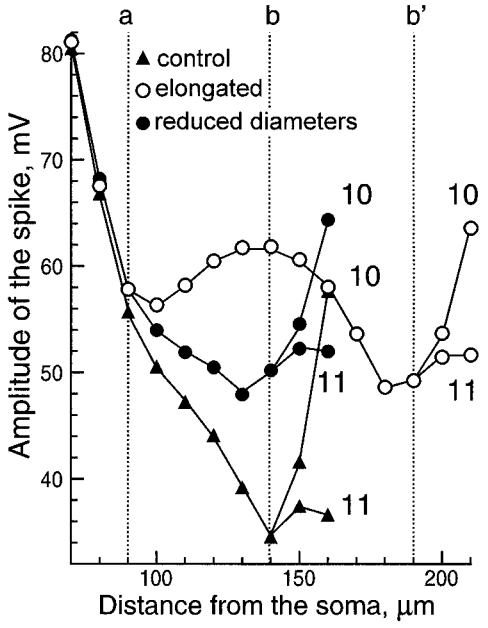


*Figure 7.* Comparison of AP amplitudes in three morphological configurations shown in Figure 6: control, with elongated branch and with decreased diameters. Part of the modeled structure included branches 3 and 9 and the first 20 $\mu$m of branches 10 and 11. Labeling of the branch points *a*, *b*, and *b'* is the same as in Figure 6. In the control (*filled triangles*), the amplitude decreased in the vicinity of branch points *a* and *b*. The amplitude was sufficient to allow active propagation into branch 10 but not into branch 11. When the distance between the two branch points was increased (*a, b', empty circles*), the amplitude of the AP was able to recover after passing the bifurcation *a* (110 $\mu$m). Approaching *b'*, the AP amplitude decreased. Active propagation, however, was achieved in both branches after *b'* (200 $\mu$m). For decreased diameters (*filled circles*), the amplitude drop was also weaker than in control, and active propagation into both collaterals (10 and 11) was observed.

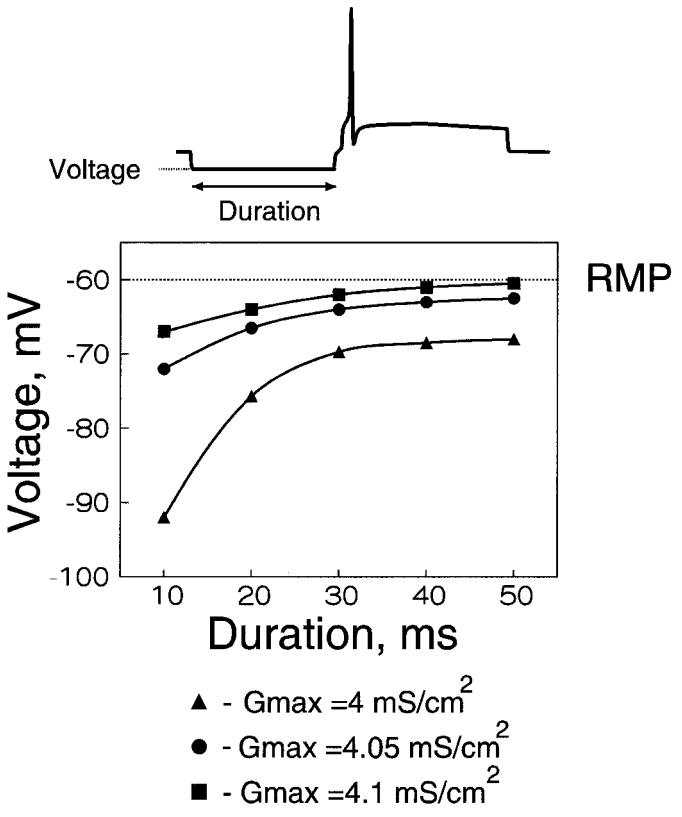


*Figure 8.* Amplitude and duration of the hyperpolarization required for the conduction failure. For different durations of the hyperpolarizing prepulse (10–50 msec), the minimal level of the hyperpolarization allowing a conduction failure was determined. Three densities of the A-channels in the hot spots were considered ($G_{A,max}$ = 4, 4.05, and 4.1 mS/cm$^2$). The hyperpolarization required for deinactivation of the A-channels decreased when the duration increased. Note the saturation for durations larger than 40 msec. The required hyperpolarization increased significantly with a small decrease in the A-channel density. For a 10 msec prepulse, hyperpolarizations deeper than −67 mV were found to be sufficient to produce a conduction block when the density at the hot spots was 4.1 mS/cm$^2$. For a smaller density of the A-channels (4.05 mS/cm$^2$), hyperpolarization had to be at least −72 mV to provide a propagation failure. With further decrease in the A-channel density (4 mS/cm$^2$), a conduction failure was obtained at −92 mV.

range and consequently induces a conduction block. This type of gating differs from previous studies (Smith, 1980) with respect to the key mechanism, although branch points also represent favorable sites for failure. We now discuss the temporal, morphological, and physiological requirements for A-current-dependent conduction block. Finally, we examine the influence of this new form of gating of AP propagation on network properties.

### Ionic channel densities and AP propagation

Successful propagation and hyperpolarization-induced conduction failure were obtained only if A-channels were clustered. With homogeneous distributions, it was not possible to reproduce experimental observations, i.e., successful propagation when the AP was elicited from RMP, *and* failure when the AP was preceded by a hyperpolarization. APs elicited from RMP failed in several branches when the density was high, and no conduction failure could be induced by the conditioning hyperpolarization when the density was low. Although these configurations do not account for the experimentally observed gating, both cases should retain attention. It is plausible that two-thirds of the CA3 cells that did not show the conduction failures (Debanne et al., 1997) corresponds to cells exhibiting low densities of A-channels. In contrast, higher density of A-channels could well account for the spontaneous conduction failures in hippocampal (Storm and Lipowsky, 1994) and cerebellar neurons (Vincent and Marty, 1996).

Despite the growing knowledge about the different subunits of the family of A-type channels (Dolly and Parcej, 1996), little is known about their precise location in the axonal membrane. A-channels have been identified in hippocampal axons through immunohistochemical techniques (Sheng et al., 1992), but their precise distribution in the axon has not been described at high resolution.

According to our findings, clustered distribution of A-channels appears crucial for this form of gating. In the hippocampus, hot spots of A-channels are found in the axons of granule cells (Cooper et al., 1998). A-channels are clustered in supraoptical neurons (Alonso and Widmer, 1997). Moreover, clustering of ionic channels in neuronal membranes has been described both experimentally (Joe and Angelides, 1992) and theoretically (Siegel et al., 1994).

One of the most important conclusions of our study is that only a few clusters of A-channels at some strategic points in the proximal axonal arborization determine whether the AP propagates. The removal of only one cluster allows normal AP conduction in the whole axonal arborization. Moreover, a small modification in A-channel density at the branch points strongly modified

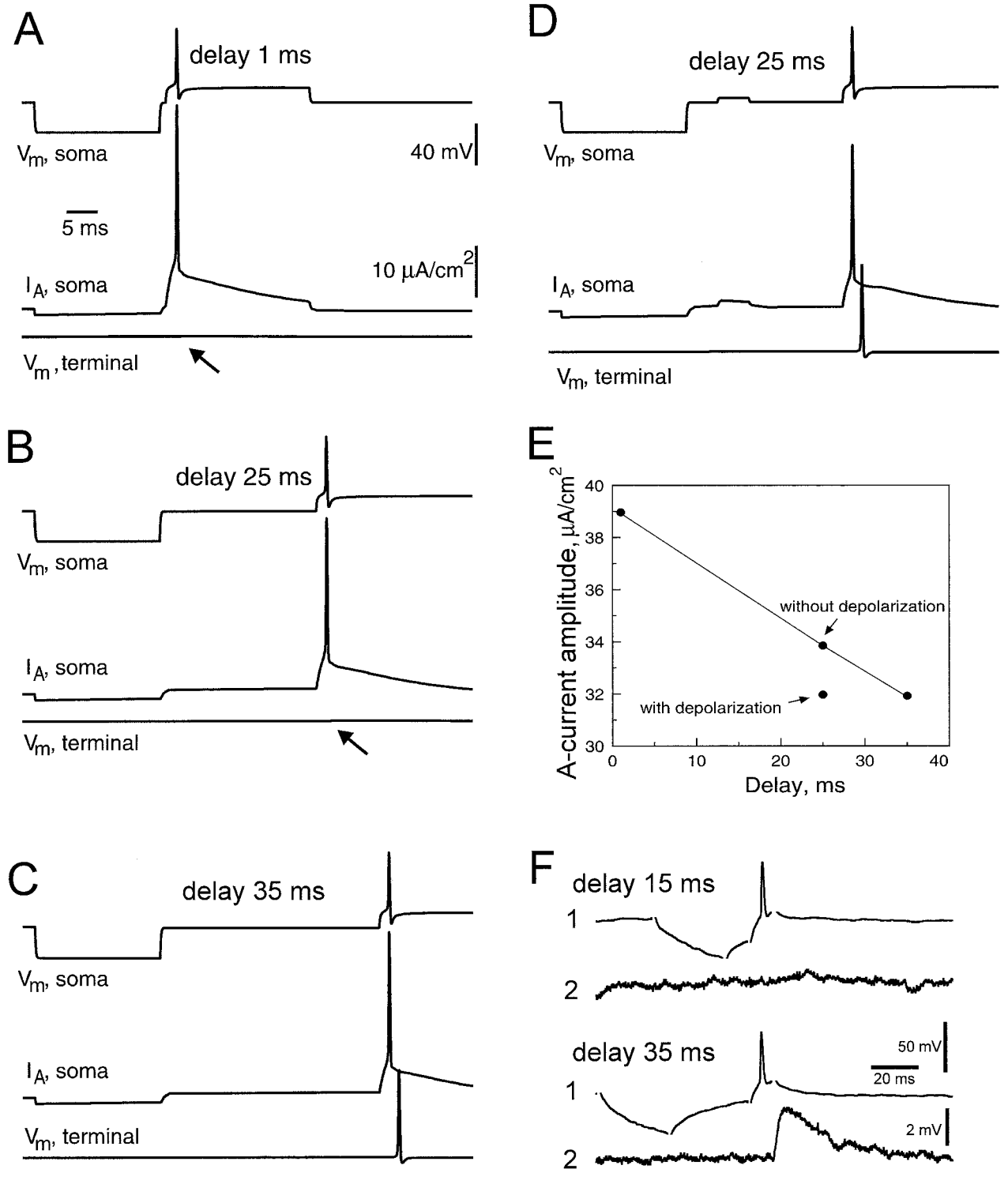


*Figure 9.* Critical delay between the hyperpolarization and AP induction ($G_{A,max}$ = 4.05 mS/cm$^2$). *A*, Time courses of the transmembrane potential ($V_{m,soma}$, *top traces*) and density of A-current ($V_{A,soma}$, *middle traces*) in the soma, and potential in terminal 16 of the principal axon ($V_{m,terminal}$, *bottom traces*) were calculated for different delays between the hyperpolarization and AP induction. Hyperpolarizing prepulse was 30 mV and its duration was 20 msec. A conduction block along the principal axon was observed when hyperpolarizing prepulse preceded the AP by 1 msec. *B*, Similar results were obtained for a delay of 25 msec. *C*, When the delay was increased to 35 msec, propagation into the principal axon was successful. *D*, When a 5 msec subthreshold depolarization was added to the configuration in *B* (25 msec delay), the AP propagated normally along the principal axon. *E*, Graph of the peak amplitude of A-current during the AP (shown in *A–D*) as a function of the delay. Note that for a delay of 25 msec, the peak amplitude was significantly reduced when a small depolarization event was added. *F*, Experimental results. Two monosynaptically coupled CA3 pyramidal cells were recorded intracellularly. When the hyperpolarizing prepulse preceded the AP by 15 msec in the cell (*1*), no EPSP was elicited in the cell (*2*). Propagation failure was not observed when the delay was increased to 35 msec.

the threshold for the conduction block (Fig. 8). This suggests that the local modulation of A-channel efficacy can regulate the output signal of the neuron in some target areas. In dendrites of hippocampal neurons, reduction of A-channel density is sufficient to modify the back-propagating AP (Hoffman et al., 1997). A-channel activity has also been reported at the presynaptic terminals (Forsythe, 1994). Their modulation can influence the presynaptic spike (Gage, 1992) and subsequently transmitter release.

When can such modulation occur? The activity of A-channels is controlled by numerous neurotransmitters such as GABA (Gage, 1992) and noradrenaline (Sah et al., 1985), chemical messengers such as $Ca^{2+}$ (Chen and Wong, 1991), cation concentration (Talukder and Harrison, 1995), auxiliary subunits (Rettig et al., 1994), and oxidative and phosphorylation states (Covarrubias et al., 1994). Thus, during the life of an axon, limited upregulations or downregulations of A-channel efficacy may strongly modify the integration capacity of the axon. One may wonder whether some developmental factors or activity-dependent patterns regulating the expression and efficacy of A-channels in the axon (Chen and Wong, 1991; Maletic-Savatic et al., 1995) allow a somatic control of the output of the cell. For example, during arousal fewer conduction failures may occur as a result of the depressing action of noradrenaline on the A-current. The cascade of events and the link between all steps remain to be determined, however.

Our results must be qualified in two important ways. We used a homogeneous distribution of $Na^+$ channels with one proximal hot spot. The presence of this hot spot has recently been reported in cultures of dissociated hippocampal cells (Dargent et al., 1998). However, this point needs to be confirmed in the organized hippocampus (organotypic cultures or acute slices). Second, because of the difficulty of recording from axons, properties of axonal channels were assumed the same as on the soma. The model showed A-current-dependent conduction blocks for a wide range of $Na^+$ channel densities. Physiologically, realistic levels of hyperpolarization required for the block were obtained, however, only for $G_{Na,max}/G_{A,max}$ ratios smaller than 12.

### Where does the failure occur?

We showed that failure could occur only if in the axon two conditions were met. The critical region had to be proximal to allow deinactivation of A-channels by the hyperpolarization, but it also had to be far enough from the area of high density of $Na^+$ channels (i.e., area of spike generation). We found that this region was in the proximal part of the axonal arborization (Fig. 4). This conclusion was corroborated by the speed at which 4-aminopyridine in the presynaptic recording pipette blocked conduction failures. The effect of the blocking agent occurred within 2 min after somatic impalement (Debanne et al., 1997).

This evaluation, however, must be qualified in three different ways. The location of AP failure was determined for a given structure and for a limited hyperpolarization (~10 mV). It is well established that changes in parameters such as axonal morphology, membrane resistivity, and amplitude of the applied hyperpolarization would modify the attenuation profiles of the steady-state voltages (Rall, 1989; Wilson, 1995).

### Temporal requirements for AP block

Two temporal parameters are critical for the A-current-dependent block of AP propagation: the duration of the preliminary hyperpolarization and the time interval between hyperpolarization and AP induction. Both parameters are determined by the time constant of A-current inactivation. These temporal requirements determine the optimal profile of the membrane potential to produce conduction failures, i.e., prolonged hyperpolarization followed by fast depolarizing transition. Our results suggest that slow IPSPs and AHPs, or summated fast IPSPs evoked at high frequency, would be more efficient than single fast IPSPs to produce conduction failure. Moreover, introduction of a subthreshold depolarization between the prepulse and the AP was sufficient to restore propagation at short delays that had not permitted conduction. This result underscores the importance of the recent history of neuronal activity for the propagation of APs along the axon. Any depolarizing event in the neuron (such as EPSPs) could accelerate the A-channel inactivation and consequently reduce the critical time interval during which A-current can induce conduction block.

### Physiological hyperpolarizations that produce conduction failures

$GABA_A$ receptor-mediated IPSP of a few millivolts blocked AP propagation both experimentally and in the simulations. It is interesting to note that the amplitude of the simulated IPSP was smaller than the threshold for conduction block when a hyperpolarization was induced by current. This apparent discrepancy resulted from the additive effect of the shunt of the chloride conductance underlying the IPSP. It further demonstrates that current injections that are usually used to mimic EPSPs or IPSPs cannot account for complex mechanisms of gating of AP propagation that involve synaptic shunting.

Other physiological hyperpolarizations such as AHPs may also produce conduction failures. Failures have been observed in cell pairs that exhibited current-induced conduction blocks when single presynaptic APs were elicited at a frequency of 1 Hz (D. Debanne, unpublished observations). Vincent and Marty (1996) reported failures of conduction in interneurons of the cerebellum firing spontaneously at a frequency of ~5–10 Hz. These failures were blocked by cesium, a nonspecific $K^+$ channel blocker. It is plausible that the AHPs that followed each AP may reset axonal A-channels and promote conduction block.

### Consequences for the function of hippocampal networks

Conduction failures mediated by A-current activation may affect the function of the hippocampal networks at several levels.

First, for two monosynaptically coupled neurons, conduction failures produce a functional disconnection, as reported by Debanne et al. (1997). This could impede, for example, Hebbian-like associative interactions that require synchronous presynaptic release of glutamate and postsynaptic depolarization. Conduction failure could also underlie apparent short-term facilitation of synaptic excitation [Storm and Lipowsky (1994); Debanne et al. (1997), their Fig. 3*b*]. When pairs of APs were elicited from a hyperpolarized potential, the first AP failed to propagate because of A-current activation. When the second AP was elicited, A-channels were inactivated by the first AP. As a result, the second AP propagated successfully. Postsynaptically, it produced an apparent strong paired-pulse facilitation that does not result from the accumulation of residual calcium in presynaptic terminals (del Castillo and Katz, 1954). The conduction properties of doublets of APs will be the subject of future simulation studies.

For a branching axon that contacts different postsynaptic neurons, it was important to show that AP failed preferentially in

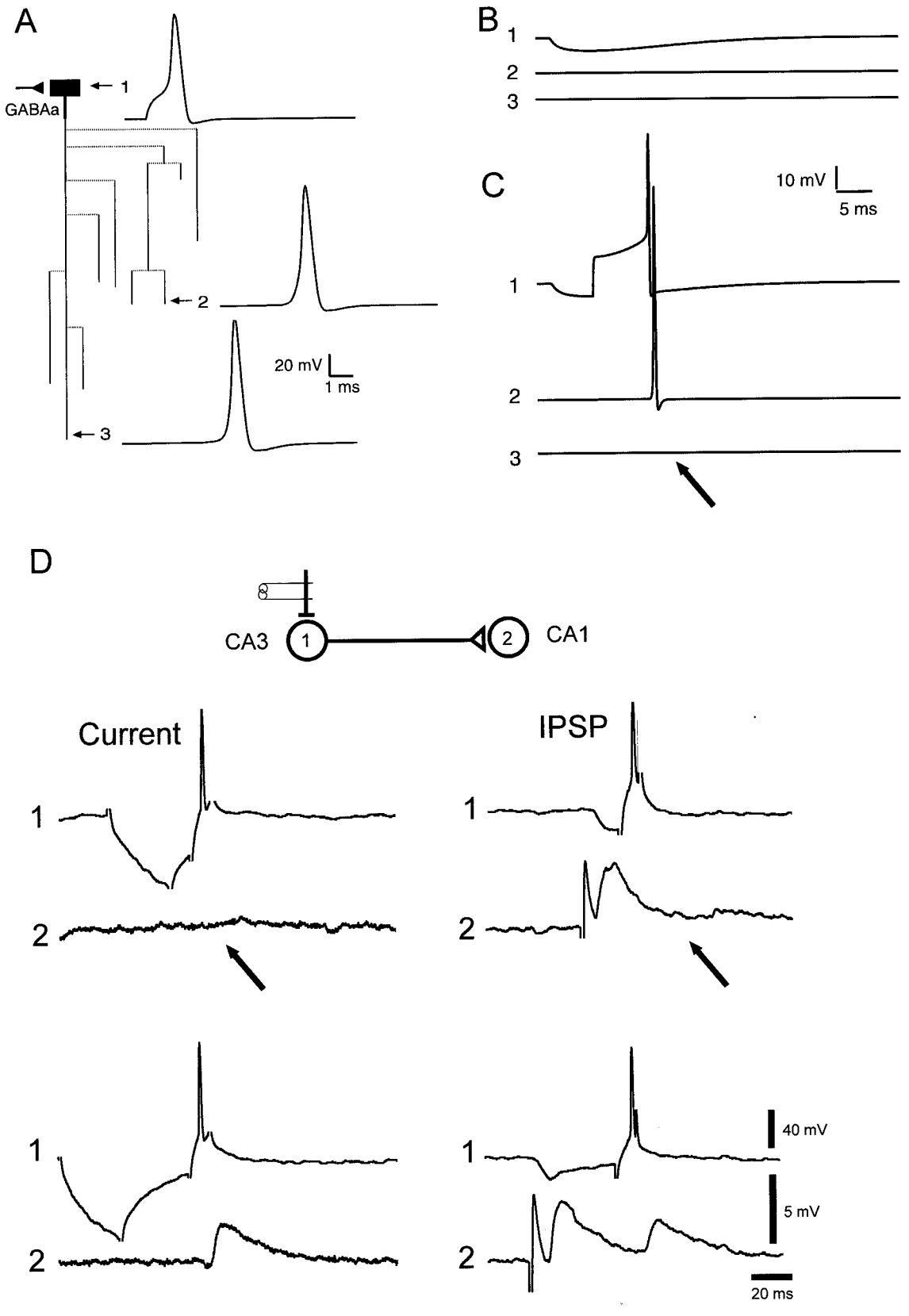


*Figure 10.* Conduction block induced by a somatic IPSP ($G_{A,max}$ = 4.05 mS/cm$^2$). *A*, $GABA_A$-receptor synaptic input was placed on the soma. Without synaptic activation, the AP elicited at the soma (*1*) propagated into both collateral (*2*) and principal axon (*3*). *B*, Membrane potentials in the soma (*1*), collateral (*2*), and principal axon (*3*) in response to activation of the synaptic input. No hyperpolarization was detected in the collateral and principal axon. *C*, The AP failed to propagate into the principal axon (*arrow* on *trace 3*) when it was elicited at the maximum of the IPSP (see *trace 1*). It was still able to propagate into the collateral (*2*). *D*, Experimental conduction block. Two pyramidal cells were recorded intracellularly (*Figure legend continues*)

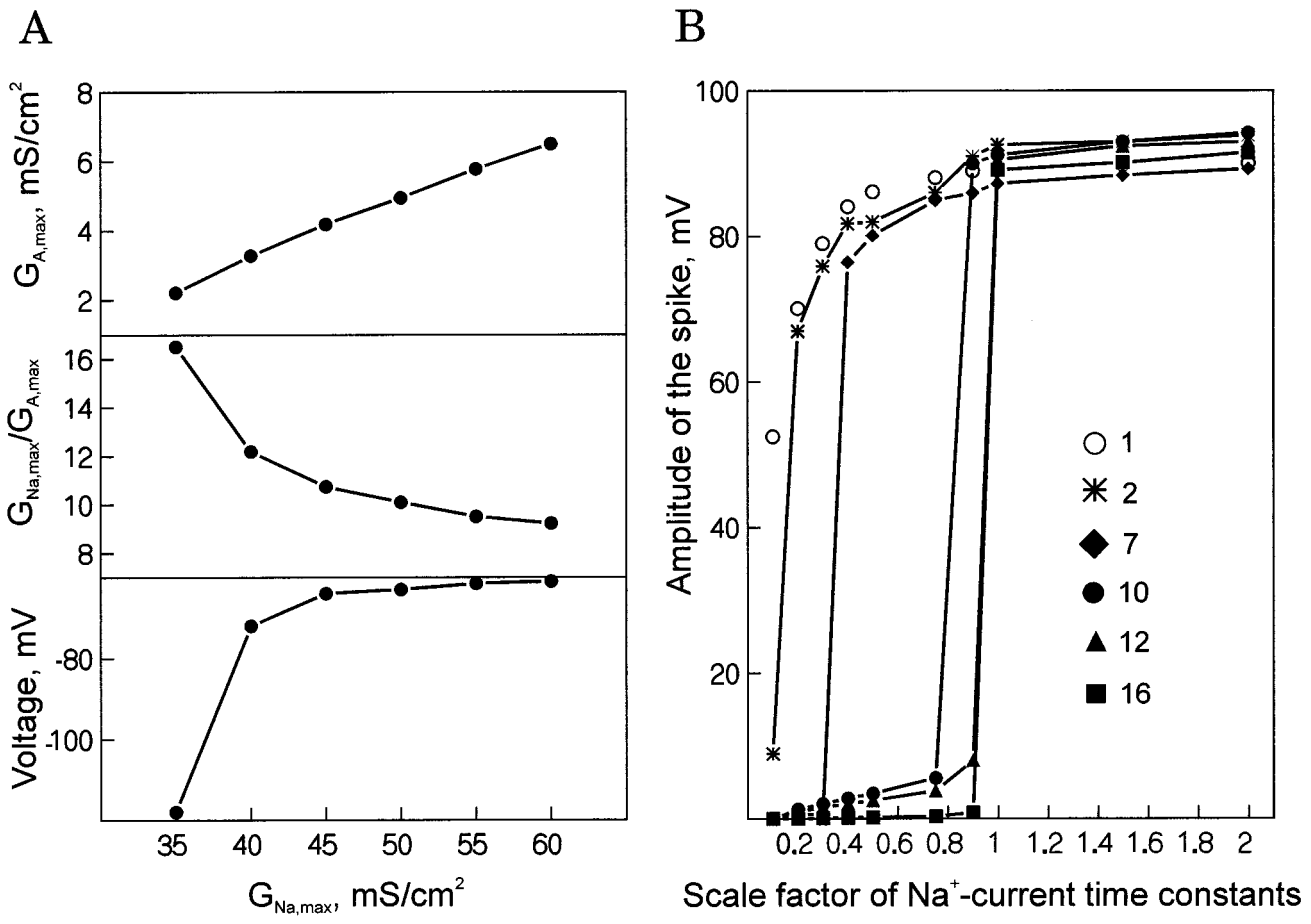


*Figure 11.* Role of the density and kinetics of $Na^+$ channels. *A*, Variation of the density. The density of $Na^+$ channels ($G_{Na,max}$) varied between 35 and 60 mS/cm$^2$ in the soma and along the axon. In the area of spike generation the density of $Na^+$ channels was 30 times higher. *Top*, The density of A-channels ($G_{A,max}$) in the hot spots was calculated from the condition of successful spike propagation into all axonal collaterals at the RMP. $G_{A,max}$ increases with the increase of $G_{Na,max}$. *Middle*, The ratio $G_{Na,max}/G_{A,max}$ was calculated from the data presented in the *top*. To higher density of $Na^+$ channels corresponded higher $G_{A,max}$ and lower $G_{Na,max}/G_{A,max}$. *Bottom*, The level of the hyperpolarization required to induce a failure of the spike propagation into the principal axon. The duration of the hyperpolarization was 20 msec. For $G_{Na,max}$ >40 mS/cm$^2$, the required level of the hyperpolarization was found to be lower than −75 mV. It suggests that for this range of $G_{Na,max}$, IPSPs or AHPs may induce conduction failures. *B*, Variation of the kinetics. For different kinetics of $Na^+$ channels the AP amplitudes in five terminals were calculated. Simulations were performed in the absence of the hyperpolarizing prepulse. The time-constants of activation and inactivation of $Na^+$ channels were multiplied by a scale factor presented on the abscissa. Scale factor equal to 1 corresponded to kinetics used in all previous simulations. For slower kinetics of $Na^+$ channels (scale factors >1), amplitudes of the AP were larger, and spikes reached all terminals. For faster kinetics, the amplitude of the AP in the area of spike generation decreased, and the AP failed to reach some (scale factors ranging between 0.2 and 0.9) or all (scale factor of 0.1) terminals.

some collaterals. Selective conduction blocks were shown to determine receptive field properties in sensory neurons of the leech (Gu, 1991). Such direct effects of propagation failures on physiological properties are difficult to establish in hippocampal formation. However, our simulations suggest that large axons that project on area CA1 [Schaffer collaterals (Li et al., 1994)] may undergo conduction failures more easily than small ones (projecting on CA3 area).

Finally, the studied phenomenon could have important consequences in the whole hippocampal network. It has been proposed that networks of interneurons entrain cortical, synchronized theta (4–7 Hz), and gamma (40 Hz) activity (Lytton and Sejnowski, 1991; Cobb et al., 1995; Whittington et al., 1995). These oscillations may produce conduction blocks because the oscillations represent the optimal condition for the deinactivation–activation sequence of A-current. In addition, activated A-current induces a delay of 0.5–1 msec in generation and conduction of the AP [Segev (1990), their Fig. 4; Debanne et al. (1997)], and it introduces timing errors in the activity of the hippocampal network. Conduction delay may increase the jitter between the input and output of the neurons (Maršàlek et al., 1997). As a result, errors in the fine temporal binding (in the millisecond range) (Bienen-

←

in areas CA3 (*1*) and CA1 (*2*). Similar effects were observed for the current-induced (*right*) and synaptically induced (*left*) hyperpolarizations of the cell (*1*). When the hyperpolarization preceded the presynaptic AP by <10 msec (*top*), no EPSP was observed postsynaptically (*arrows*). When the delay between the hyperpolarizing prepulse and the presynaptic AP was >30 msec (*bottom*), an EPSP was elicited for both types of hyperpolarization, indicating normal AP conduction into the presynaptic axon. The complex response before the unitary EPSP in the cell (*2*) resulted from activation of Schaffer collaterals.

stock, 1995) would be introduced. The precise consequences of such perturbations on the composition of cognitive functions remain to be determined.

## APPENDIX

The transmembrane voltage $V$ along the modeled structure was calculated solving the cable equation numerically:

$$\partial(a(x)/2R_i \cdot \partial V/\partial x)/\partial x = C_m \cdot \partial V/\partial t + I_m(V, t) + I_{syn}(V, t) + I_{inj}(t), \quad (A1)$$

where $x$ is a coordinate and $a(x)$ the diameter of the structure. $C_m$ denotes the capacity per unit area (1 $\mu$F/cm$^2$). $R_i$ is the resistivity of the cytoplasm (100 $\Omega \cdot$ cm). $I_m$, $I_{syn}$, and $I_{inj}$ are densities of transmembrane ionic current, postsynaptic current, and polarizing current injected in the first compartment of the soma, respectively.

For each compartment of the soma, $I_m$ was represented as:

$$I_m = I_{Na} + I_K + I_{Ca} + I_{K(Ca)} + I_{C(Ca)} + I_A + I_{leak}, \quad (A2)$$

and for each compartment of the axon as:

$$I_m = I_{Na} + I_K + I_A + I_{leak}, \quad (A3)$$

where $I_{Na}$ denotes the current through excitable $Na^+$ channels, $I_K$ the delayed rectifier $K^+$ current, $I_{Ca}$ the $Ca^{2+}$ current, $I_A$ the A-type $K^+$ current, $I_{K(Ca)}$ the long-duration $Ca^{2+}$-dependent $K^+$ current, $I_{C(Ca)}$ the short-duration voltage-dependent and $Ca^{2+}$-dependent $K^+$ current, and $I_{leak}$ the leak current.

Each of the active components of the transmembrane current was described by a modified Hodgkin-Huxley-type equation (Traub et al., 1991; Pongracz et al., 1992):

$$I_{Na} = G_{Na,max} \cdot m^3 \cdot h \cdot (V - V_{Na}), \quad (A4)$$

$$I_K = G_{K,max} \cdot n^4 \cdot (V - V_K), \quad (A5)$$

$$I_{Ca} = G_{Ca,max} \cdot s \cdot r \cdot (V - V_{Ca}), \quad (A6)$$

$$I_A = G_{A,max} \cdot a \cdot b \cdot (V - V_K), \quad (A7)$$

$$I_{K(Ca)} = G_{K(Ca),max} \cdot q \cdot (V - V_K), \quad (A8)$$

$$I_{C(Ca)} = G_{C(Ca),max} \cdot c \cdot \min[1, 0.0663 \cdot ([Ca^{2+}]_i/[Ca^{2+}]_{i,max})] \cdot (V - V_K), \quad (A9)$$

where $G_{ion,max}$ is the maximum value for the corresponding kind of ionic conductances: $Na^+$, $K^+$, $Ca^{2+}$, A-type, $Ca^{2+}$-dependent $K^+$, and fast $Ca^{2+}$-dependent $K^+$. Their values are given in Material and Methods and in Table 2. *m, n, s, r, a, b*, and *c* are voltage-dependent variables, and $q$ is a $Ca^{2+}$-dependent state variable of activation and inactivation of the corresponding conductances. Their dynamics were given by the differential equation:

$$di/dt = \alpha_i \cdot (1 - i) - \beta_i \cdot i, \quad (A10)$$

with the same rate constants $\alpha_i$ and $\beta_i$ for *m, h, n, s, r, q*, and *c* as in Pongracz et al. (1992) (Table 2) and Traub et al. (1991) (Tables 1, 2) for *a* and *b*.

Reversal potentials (relative to the RMP of −60 mV) for $Na^+$ ($V_{Na}$), $K^+$ ($V_K$), and $Ca^{2+}$ ($V_{Ca}$) were 115, −15, and 140 mV, respectively.

The kinetics of $[Ca^{2+}]_i$ in the somatic compartments was described by Equation 17 from Pongracz et al. (1992).

Leakage current $I_{leak}$ was determined as:

$$I_{leak} = G_{leak} \cdot (V - V_{leak}), \quad (A11)$$

where $V_{rest}$ was 0 mV, and leakage conductance $G_{leak}$ was calculated for each compartment of the structure from the condition that at the resting state total transmembrane current equals zero.

Hyperpolarization was induced either by injection of the step of the current $I_{inj}$ on the soma or by activation of the somatic $GABA_A$ synaptic inputs. Postsynaptic current $I_{syn}$ was presented as:

$$I_{syn} = G_{syn} \cdot (V - V_{Cl}), \quad (A12)$$

with $V_{Cl}$, the reversal potential for $Cl^-$, set to −10 mV relative to the RMP and $G_{syn}$ as an $\alpha$-function (Bernander et al., 1994):

$$G_{syn} = G_{syn,max} \cdot e/t_{peak} \cdot t \cdot e^{-t/t_{peak}} \quad (A13)$$

with a time-to-peak, $t_{peak}$ of 6 msec, in accordance with experimental data (Miles, 1990; Debanne et al., 1995).

## REFERENCES


Alonso G, Widmer H (1997) Clustering of Kv4.2 potassium channels in supraoptic membrane of rat supraoptic neurons: an ultrastructural study. Neuroscience 77:617–621.

Andersen P, Silfvenius H, Sundberg SH, Sveen O, Wigström H (1978) Functional characterization of unmyelinated fibres in the hippocampal cortex. Brain Res 144:11–18.

Bernander O, Koch C, Douglas RJ (1994) Amplification and linearization of distal synaptic input to cortical pyramidal cells. J Neurophysiol 72:2743–2753.

Bielefeldt K, Jackson MB (1993) A calcium-activated potassium channel causes frequency-dependent action potential failures in a mammalian nerve terminal. J Neurophysiol 70:284–298.

Bienenstock E (1995) A model of neocortex. Network 6:179–224.

Bossu J-L, Capogna M, Debanne D, McKinney RA, Gähwiler BH (1996) Somatic voltage-gated potassium currents of rat hippocampal pyramidal cells in organotypic slice cultures. J Physiol (Lond) 495:367–381.

Chen QX, Wong RKS (1991) Intracellular $Ca^{2+}$ suppressed a transient potassium current in hippocampal neurons. J Neurosci 11:337–343.

Cobb SR, Buhl EH, Halasy K, Paulsen O, Somogyi P (1995) Synchronization of neuronal activity in hippocampus by individual GABAergic interneurons. Nature 378:75–78.

Colbert CM, Johnston D (1996) Axonal action-potential initiation and $Na^+$ channel densities in the soma and axon initial segment of subicular pyramidal neurons. J Neurosci 16:6676–6686.

Cooper EC, Milroy A, Jan YN, Jan LY, Lowenstein DH (1998) Presynaptic localization of Kv 1.4-containing A-type potassium channels near excitatory synapses in the hippocampus. J Neurosci 18:965–974.

Covarrubias M, Wei A, Salkoff L, Vyas TB (1994) Elimination of rapid potassium channel inactivation by phosphorylation of the inactivation gate. Neuron 13:1403–1412.

Dargent B, Mouret I, Shah RM, Spooner ET, Boudier JA, Le Bivic A, Mane R, Sampo B (1998) Targeting of the voltage-dependent sodium channel to the axon of cultured hippocampal neurons. Soc Neurosci Abstr, in press.

Debanne D, Guérineau NC, Gähwiler BH, Thompson SM (1995) Physiology and pharmacology of unitary synaptic connections between pairs of cells in areas CA3 and CA1 of rat hippocampal slice cultures. J Neurophysiol 73:1282–1294.

Debanne D, Guérineau NC, Gähwiler BH, Thompson SM (1997) Action-potential propagation is gated by an $I_A$-like potassium conductance in hippocampus. Nature 389:286–289.

del Castillo J, Katz B (1954) Statistical factors involved in neuromuscular facilitation and depression. J Physiol (Lond) 124:574–585.

Dolly JO, Parcej DN (1996) Molecular properties of voltage-gated $K^+$ channels. J Bioenerg Biomembr 28:231–253.

Forsythe ID (1994) Direct patch recording from identified presynaptic

terminals mediating glutamatergic EPSCs in the rat CNS, in vitro. J Physiol (Lond) 479:381–387.
Frotscher M, Gähwiler BH (1988) Synaptic organization of intracellularly stained CA3 pyramidal neurons in slice cultures of rat hippocampus. Neuroscience 24:541–551.
Gage PW (1992) Activation and modulation of neuronal $K^+$ channels by GABA. Trends Neurosci 15:46–51.
Gähwiler BH (1981) Organotypic monolayer cultures of nervous tissue. J Neurosci Methods 4:329–342.
Graham B, Redman S (1994) A simulation of action potentials in synaptic boutons during presynaptic inhibition. J Neurophysiol 71:538–549.
Grossman Y, Parnas I, Spira MK (1979a) Differential conduction block in branches of a bifurcating axon. J Physiol (Lond) 295:283–305.
Grossman Y, Parnas I, Spira MK (1979b) Ionic mechanisms involved in differential conduction of action potentials at high frequency in a branching axon. J Physiol (Lond) 295:307–322.
Gu X (1991) Effect of conduction block at axon bifurcations on synaptic transmission to different postsynaptic neurones in the leech. J Physiol (Lond) 441:755–778.
Hoffman DA, Magee JC, Colbert CM, Johnston D (1997) $K^+$ channel regulation of signal propagation in dendrites of hippocampal pyramidal neurons. Nature 387:869–875.
Ishizuka N, Weber J, Amaral DG (1990) Organization of intrahippocampal projections originating from CA3 pyramidal cells in the rat. J Comp Neurol 295:580–623.
Jackson MB, Zhang SJ (1995) Action potential propagation and propagation block by GABA in rat posterior pituitary nerve terminals. J Physiol (Lond) 483:597–611.
Joe E, Angelides K (1992) Clustering of voltage-dependent sodium channels on axons depends on Schwann cell contact. Nature 356:333–335.
Joyner RW, Westerfield M, Moore JW (1980) Effects of cellular geometry on current flow during a propagated action potential. Biophys J 31:183–194.
Klee R, Ficker E, Heinemann U (1995) Comparison of voltage-dependent potassium currents in rat pyramidal neurons acutely isolated from hippocampal regions CA1 and CA3. J Neurophysiol 74:1982–1995.
Kopysova IL, Korogod SM (1989) Studies of non-uniform fragments of the neuronal membranes with the use of the subject-oriented program tool. In: Application of the computations and mathematical methods in scientific investigations (Antomonov B, ed), pp 127–128. Kiev: Naukova Dumka.
Kosaka T (1980) The axon initial segment as a synaptic site: ultrastructure and synaptology of the initial segment of the pyramidal cell in the rat hippocampus (CA3 region). J Neurocytol 9:861–882.
Korogod SM (1989) Synthesis of mathematical models of branching axons and dendrites. Neurophysiology (Kiev) 20:343–350.
Korogod SM, Ivanov YN, Kopysova IL, Kukushka VI (1991) Application of neuroscience oriented simulation software program to studies of synaptic interactions in anatomically and biophysically complex neurones. J Physiol (Lond) 438:286P.
Korogod SM, Bras H, Sarana VN, Gogan P, Tyc-Dumont S (1994) Electrotonic clusters in the dendritic arborization of abducens motoneurons of the rat. Eur J Neurosci 6:1517–1527.
Li X-G, Somogyi P, Ylinen A, Buszáki G (1994) The hippocampal CA3 network: an in vivo intracellular labeling study. J Comp Neurol 339:181–208.
Lüscher H-R, Shiner JS (1990) Simulation of action potential propagation in complex terminal arborizations. Biophys J 58:1389–1399.
Lüscher C, Streit J, Quadroni R, Lüscher H-R (1994a) Action potential propagation through embryonic dorsal root ganglion cells in culture. I. Influence of the cell morphology on propagation properties. J Neurophysiol 72:622–633.
Lüscher C, Streit J, Lipp P, Lüscher H-R (1994b) Action potential propagation through embryonic dorsal root ganglion cells in culture. II. Decrease of conduction reliability during repetitive stimulation. J Neurophysiol 72:634–643.
Lüscher C, Lipp P, Lüscher H-R, Niggli E (1996) Control of action potential propagation by intracellular $Ca^{2+}$ in cultured rat dorsal root ganglion cells. J Physiol (Lond) 490:319–324.
Lytton WW, Sejnowski TJ (1991) Simulations of cortical pyramidal neurons synchronized by inhibitory interneurons. J Neurophysiol 66:1059–1079.
Maletic-Savatic M, Lenn NJ, Trimmer JS (1995) Differential spatiotemporal expression of $K^+$ channel polypeptides in rat hippocampal neurons developing *in situ* and *in vitro*. J Neurosci 15:3840–3851.
Maršàlek P, Koch C, Maunsell J (1997) On the relationship between synaptic input and spike output jitter in individual neurons. Proc Natl Acad Sci USA 94:735–740.
Miles R (1990) Variation in strength of inhibitory synapses in the CA3 region of guinea-pig hippocampus in vitro. J Physiol (Lond) 431:659–676.
Nicoll RA, Alger BE (1979) Presynaptic inhibition: transmitter and ionic mechanisms. Int Rev Neurobiol 21:217–258.
Numann RE, Wadmann WJ, Wong RKS (1987) Outward currents of single hippocampal cells obtained from the adult guinea-pig. J Physiol (Lond) 393:331–353.
Parnas I (1972) Differential block at high frequency of branches of a single axon innervating two muscles. J Neurophysiol 35:903–914.
Parnas I, Hochstein S, Parnas H (1976) Theoretical analysis of parameters leading to frequency modulation along an inhomogeneous axon. J Neurophysiol 39:909–923.
Pongracz F, Poolos NP, Kocsis JD, Shepherd GM (1992) A model of NMDA receptor-mediated activity in dendrites of hippocampal CA1 pyramidal neurons. J Neurophysiol 68:2248–2259.
Rall W (1989) Cable theory for dendritic neurons. In: Methods in neuronal modeling (Koch C, Segev I, eds), pp 9–62. Cambridge, MA: MIT.
Ramon y Cajal S (1911) Histologie du système nerveux central de l'homme et des vertébrés. Paris: Maloine.
Rapp M, Yarom Y, Segev I (1996) Modeling back propagating action potential in weakly excitable dendrites of neocortical pyramidal cells. Proc Natl Acad Sci USA 93:11985–11990.
Rettig J, Heinemann SH, Wunder F, Lorra C, Parcej DN, Dolly JO, Pongs O (1994) Inactivation properties of voltage-gated $K^+$ channels altered by presence of $\beta$-subunit. Nature 369:289–294.
Sah P, French CR, Gage PW (1985) Effects of noradrenaline on some potassium currents in CA1 neurones in rat hippocampal slices. Neurosci Lett 60:295–300.
Sah P, Gipp AJ, Gage PW (1988) Potassium current activated by depolarization of dissociated neurons from adult guinea pig hippocampus CA1 neurons. J Gen Physiol 92:263–278.
Segal M, Rogawski MA, Baker JL (1984) A transient potassium conductance regulates the excitability of cultured hippocampal and spinal neurons. J Neurosci 4:604–609.
Segev I (1990) Computer study of presynaptic inhibition controlling the spread of action potentials into axonal terminals. J Neurophysiol 63:987–998.
Sheng M, Tsaur M-L, Jan YN, Jan LY (1992) Subcellular segregation of two A-type $K^+$ channel protein in rat central neurons. Neuron 9:271–284.
Siegel M, Marder E, Abbott F (1994) Activity-dependent current distributions in model neurons. Proc Natl Acad Sci USA 91:11308–11312.
Smith DO (1980) Mechanisms of action potential propagation failure at sites of axon branching in the crayfish. J Physiol (Lond) 301:243–259.
Storm JF (1990) Potassium currents in hippocampal pyramidal cells. Prog Brain Res 83:161–187.
Storm JF, Lipowsky R (1994) Evidence that excitability changes in presynaptic fibers may affect paired-pulse facilitation in hippocampal slices. Soc Neurosci Abstr 20:1339.
Talukder G, Harrison NL (1995) On the mechanism of modulation of transient outward current in cultured rat hippocampal neurons by di- and trivalent cations. J Neurophysiol 73:73–79.
Traub RD, Wong RKS, Miles R, Michelson H (1991) A model of a CA3 hippocampal pyramidal neuron incorporating voltage-clamp data on intrinsic conductances. J Neurophysiol 66:635–650.
Traub RD, Jefferys JGR, Miles R, Whittington MA, Tóth K (1994) A branching dendritic model of a rodent CA3 pyramidal neurone. J Physiol (Lond) 481:79–95.
Vincent P, Marty A (1996) Fluctuations of inhibitory postsynaptic currents in Purkinje cells from rat cerebellar slices. J Physiol (Lond) 494:183–199.
Wall, PD (1995) Do nerve impulses penetrate terminal arborizations? A pre-presynaptic control mechanism. Trends Neurosci 18:99–103.
Westrum LE, Blackstad TW (1962) An electron microscopic study of the stratum radiatum of the rat hippocampus (regio superior, CA1) with particular emphasis on synaptology. J Comp Neurol 119:281–309.
Whittington MA, Traub RD, Jefferys JGR (1995) Synchronized oscillations in interneuron networks driven by metabotropic glutamate receptor activation. Nature 373:612–615.
Wilson CJ (1995) Dynamic modification of dendritic cable properties and synaptic transmission by voltage-gated potassium channels. J Comput Neurosci 2:91–115.